How and Why Do Bremsstrahlung Radiation have Unstructured Wavefronts

Mert Yucemoz[1]

[1]Affiliation not available

March 10, 2026

Abstract

This article extends the mathematical model of the complete radiation patterns of the bremsstrahlung process, which involves bremsstrahlung asymmetry and Doppler shift. Firstly, the mathematical model is simplified, preserving the forward-backward peaking radiation properties and the involved asymmetries. This helped investigate and model the tendency of rotation in the wavefront of the emitted wave. Consequently, it has been found that the curl of the gradient of the radiation intensity is non-zero and the wavefront of the bremsstrahlung radiation follows a tapered spiral wavefront. The radius of the rotational wavefront was found to decrease as the wave propagates. The spiral geometry has different magnitudes of radius with respect to the direction of particle motion as the wavefront rotates. Hence, the different magnitudes of spiral wavefronts in 2D are the result of the involved bremsstrahlung and Doppler shift asymmetries. This is also supported diagrammatically by applying Huygens's principle to a relativistic radiation pattern. This is supported by the quantization of the bremsstrahlung asymmetry, R, through momentum transfer from the particle to the rotating wavefront photon, which is quantized via conservation of momentum. In addition to three different concepts (Huygens's principle, Quantization of R, Curl) used to model the bremsstrahlung wavefront, the fourth novel concept of rewriting the alpha quantity inside bremsstrahlung asymmetry, R for even denominator R values, meaning taking the square root of a negative number, allowed to extend the model to describe the phase structure of the wave. All four different concepts agree on the predicted wavefront. The wavefront of Bremsstrahlung emissions starts at the forward lobe with a rotating and irregularly shrinking radius wavefront. When the rotation of the wavefront crosses from the forward to the backward lobe, it passes through the origin where the particle is located. This process repeats until the wavefront rotation collapses into an adjacent dipole pattern.

Journal of Physics Communications

Crossmark

PAPER

How and Why Do Bremsstrahlung Radiation have Unstructured Wavefronts

RECEIVED
dd Month yyyy

REVISED
dd Month yyyy

Mert Yücemöz [1]

[1]Department, Institution, City, Country

*Author to whom any correspondence should be addressed.

E-mail: mert.yucemoz@alumni.cern

Keywords: Bremsstrahlung process, Rotational Wavefront, Huygen's Principle, Quantised Bremsstrahlung Asymmetry

Key Points

- Novel fractional decomposition of Bremsstrahlung Asymmetry, R inside parameter α led to a novel formula ($\Phi(\theta_{n,\beta},\varphi) = y^2\Upsilon\sin(R\varphi)$) defining the phase structure of the forward-backward peaking asymmetric bremsstrahlung radiation patterns.
- Discrete values of bremsstrahlung asymmetry, R introduces physical discontinuity causing curl of a gradient of radiation intensity field to be non-zero $\left(\boldsymbol{\nabla}\times\nabla\frac{d^2I}{d\omega\Omega_{rad}}\neq 0\right)$.

Abstract

This article extends the mathematical model of the complete radiation patterns of the bremsstrahlung process, which involves bremsstrahlung asymmetry and Doppler shift. Firstly, the mathematical model is simplified, preserving the forward-backward peaking radiation properties and the involved asymmetries. This helped investigate and model the tendency of rotation in the wavefront of the emitted wave. Consequently, it has been found that the curl of the gradient of the radiation intensity is non-zero and the wavefront of the bremsstrahlung radiation follows a tapered spiral wavefront. The radius of the rotational wavefront was found to decrease as the wave propagates. The spiral geometry has different magnitudes of radius with respect to the direction of particle motion as the wavefront rotates. Hence, the different magnitudes of spiral wavefronts in 2D are the result of the involved bremsstrahlung and Doppler shift asymmetries. This is also supported diagrammatically by applying Huygens's principle to a relativistic radiation pattern. This is supported by the quantization of the bremsstrahlung asymmetry, R, through momentum transfer from the particle to the rotating wavefront photon, which is quantized via conservation of momentum. In addition to three different concepts (Huygens's principle, Quantization of R, Curl) used to model the bremsstrahlung wavefront, the fourth novel concept of rewriting the alpha quantity inside bremsstrahlung asymmetry, R for even denominator R values, meaning taking the square root of a negative number, allowed to extend the model to describe the phase structure of the wave. All four different concepts agree on the predicted wavefront. The wavefront of Bremsstrahlung emissions starts at the forward lobe with a rotating and irregularly shrinking radius wavefront. When the rotation of the wavefront crosses from the forward to the backward lobe, it passes through the origin where the particle is located. This process repeats until the wavefront rotation collapses into an adjacent dipole pattern.

1 Introduction

Radiation can be understood in terms of wavefronts, surfaces of equal phase that describe how the wave propagates. When radiation is coherent, its wavefront remains stable and aligned in both space and time. This coherence is what allows structured beams, such as those carrying orbital angular momentum (OAM), to maintain a helical wavefront. In such beams, photons all share the same quantized angular momentum state ($\ell\hbar$), producing a corkscrew-like twist that persists over

distance [1]. Unlike normal light, which has only two fundamental spin angular momentum states (polarization: left or right circular), twisted light can occupy infinitely many OAM states labeled by integers ℓ = ... -3, -2, -1, 0, 1, 2, 3.... Each ℓ corresponds to a unique twist of the wavefront. This makes twisted light a powerful tool for encoding information(assigning symbols to different ℓ values) and for probing material properties, especially chirality [2].

A growing body of high energy and research on how matter behaves when it is exposed to extremely intense electric, magnetic, or electromagnetic fields, fields so strong that they push electrons into nonlinear motion and allow radiation processes that do not occur under ordinary conditions. In these extreme environments, circularly polarized light can transfer its spin to the emitted photons, producing high-energy radiation with a helical phase structure (strong field) research shows that orbital angular momentum (OAM) can arise naturally in several fundamental radiation processes. In nonlinear Compton scattering, strong field Quantum electrodynamics (QED) predicts that circularly polarized laser fields can convert spin angular momentum into the azimuthal phase of emitted γ photons, producing high-energy vortex radiation [3]. Related strong field theory demonstrates that the nonlinear Breit - Wheeler process can generate ultra relativistic electrons and positrons with large intrinsic OAM, indicating that pair-production cascades can naturally populate vortex leptons in extreme electromagnetic environments [4]. At the atomic scale, Bethe–Heitler bremsstrahlung from vortex electrons produces photons with OAM dependent angular distributions, showing that scattering in Coulomb fields can imprint azimuthal structure on emitted radiation [5]. Classical analogues include nonlinear Thomson scattering from relativistic electrons driven by structured electromagnetic fields generates radiation with controllable OAM orientation [6]. Nonlinear optical processes also contribute high harmonic generation multiplies the OAM of the driving field into the extreme-ultraviolet regime [7], while inverse Compton scattering from twisted (Bessel) electrons can synthesize spatially structured X-ray beams whose profiles and topological charge are determined by the OAM and opening angle of the incident electron state [8]. Plasma mediated mechanisms further support OAM transfer via stimulated Raman scattering which can amplify and generate twisted electromagnetic pulses in laser driven plasmas [9]. In addition, exact OAM carrying eigenmodes photons, phonons, and plasmons have been derived in unmagnetized homogeneous plasmas, where the distribution of OAM among electrons, ions, and fields depends on charge polarity and mode type [10]. Finally, synchrotron like mechanisms extend into the X-ray domain: radiation from a single electron in circular motion has been shown to possess a helical phase structure directly associated with OAM, confirming that free-electron curvature radiation can naturally carry orbital angular momentum [11]. Collectively, these results demonstrate that OAM is not restricted to engineered optical systems but emerges naturally across a wide range of high-energy radiation processes.

Wang et al. (2022) showed within a full QED treatment that bremsstrahlung can naturally generate orbital angular momentum in the emitted photon and also in the scattered electron. In the process $e^-_{\text{in}} \rightarrow e^-_{\text{out}} + \gamma_{\text{out}}$ they constructed vortex-state wavefunctions for the final particles and calculated the corresponding differential cross section. The appearance of angular momentum dependent Kronecker symbols in their expression demonstrates how spin angular momentum (SAM) and orbital angular momentum (OAM) are exchanged during scattering while conserving total angular momentum. Their numerical analysis further shows that the angular distribution of the emitted radiation contains OAM dependent structure absent in classical plane-wave bremsstrahlung, indicating that curved-trajectory electron scattering can imprint azimuthal phase information onto the photon field [12].

A helical undulator is a magnetic structure that forces relativistic electrons to follow a helical trajectory, causing their acceleration vector to rotate continuously. Because electromagnetic radiation is emitted in the direction of the instantaneous acceleration, this rotating motion imprints an azimuthal phase structure on the emitted synchrotron radiation. Bahrdt et al. (2013) provided the first direct experimental confirmation that such spiraling electrons emit photons carrying orbital angular momentum (OAM). To detect the OAM, the authors superimposed the OAM carrying photon beam with a reference beam that had no OAM. The reference beam acts only as a phase probe, when a vortex beam interferes with a flat phase beam, the resulting intensity pattern forms a spiral whose handedness reveals the sign of the OAM. This does not mean that OAM is transferred to the reference beam; rather, the spiral interference pattern is the standard diagnostic proving that the original photon beam itself carries OAM. The observed spiral structure matched numerical simulations with excellent agreement, confirming that the emitted radiation possessed a well-defined azimuthal phase dependence. This experiment establishes a general physical principle: whenever electrons follow curved, helical, or rotating trajectories, the emitted radiation naturally acquires rotating, OAM like wavefronts. This principle is directly

relevant to natural environments, because lightning-accelerated electrons follow curved, branching, and sometimes spiral paths, runaway electrons in TGFs propagate along curved electric field lines, and bremsstrahlung from curved trajectories exhibits the same angular momentum structure. Thus, the undulator experiment serves as a controlled laboratory analogue demonstrating how OAM bearing electromagnetic fields can arise naturally without engineered optics [13].

Transition radiation is emitted when a charged particle crosses the boundary between two media. Although the electron's trajectory is rectilinear, the sudden change in electromagnetic boundary conditions produces radiation with a rich angular structure. The researchers experimentally demonstrated that transition radiation can carry orbital angular momentum (OAM) [14]. In their setup, 220 MeV electrons struck an Au-coated Si wafer, generating transition radiation whose spatial phase structure was analyzed. The authors observed that the emitted photons exhibited the characteristic signatures of twisted light, confirming that OAM can arise even without any helical or curved electron motion. This result shows that OAM generation does not require spiraling trajectories; instead, it can emerge from the interaction of relativistic electrons with material boundaries, where the discontinuity in the electromagnetic field imposes an azimuthal phase structure on the emitted radiation. These findings extend the family of natural OAM producing mechanisms and reinforce the broader principle that high-energy electron interactions whether curved or rectilinear can imprint twist like structure on emitted electromagnetic waves.

This finding suggests a potential relevance to atmospheric high energy processes. Lightning accelerated electrons propagate through regions with sharp plasma gradients, strong Coulomb scattering, and rapidly varying electric fields, conditions that may act as natural analogues to the electromagnetic discontinuities that generate OAM in transition radiation. While the environments differ, the underlying principle that abrupt changes in the electromagnetic field can imprint azimuthal structure on emitted radiation indicates a plausible pathway by which lightning bremsstrahlung could exhibit OAM like features.

Epp, Guselnikova, and Janz (2024) analyzed the angular momentum content of radiation emitted by an ultra-relativistic charge moving along an arbitrary trajectory, with special attention to the instantaneous center of curvature. They derived explicit expressions for the angular distribution of angular momentum flux and showed that the radiation naturally decomposes into components associated with the curvature of the trajectory. Their results demonstrate that curved electron motion inherently produces radiation with non trivial angular momentum structure, including azimuthal components analogous to those used to describe OAM like wavefronts. This provides a theoretical foundation for understanding how curvature driven processes common in astrophysical plasmas and potentially relevant in atmospheric high-energy environments—can generate radiation with structured angular momentum [15].

Atmospheric turbulence introduces random refractive index fluctuations that distort the phase structure of an engineered OAM beam as it propagates. These distortions can degrade the helical wavefront and induce coupling between different OAM modes, reducing the purity and stability of the transmitted state [16]. Understanding how turbulence modifies the spatial and phase structure of such structured light fields is therefore essential for predicting long-range performance and for designing robust free-space optical systems.

While OAM beams used in terrestrial experiments are engineered, several authors have proposed that astrophysical processes such as scattering near compact objects [17] or interactions with rotating gravitational fields could imprint orbital angular momentum on natural light [18]. This possibility motivates the broader question of whether OAM bearing fields might arise in other physical environments as well. In this context, this research examines the bremsstrahlung process as a potential natural mechanism capable of generating temporary structured wavefronts with OAM like characteristics and evaluates how such fields would behave during propagation. Regardless of origin, atmospheric turbulence plays a critical role in determining how an OAM beam evolves over long distances, making it essential to understand both engineered and potentially natural sources within the same propagation framework.

Lightning sferics have been increasingly studied as probes of the Earth ionosphere system and as tools for lightning mapping. Analyzed instantaneous phase and frequency of sferics inferred from complex waveforms, demonstrating how sferics can act as natural probes of the lower ionosphere and revealing perturbations linked to atmospheric chemistry and space weather events [19]. Literature emphasized the diagnostic potential of the "coherency" analysis for ionospheric monitoring and demonstrated that lightning sferics can act as natural probes for ionospheric electron density changes. Propagation characteristics of lightning sferics within the Earth–ionosphere waveguide, identifying attenuation and dispersion patterns that directly affect coherency and underscoring the importance of propagation modeling for accurate lightning location

[20]. These results provide a foundation for improving long-range lightning detection networks by accounting for waveguide effects [21]. The electromagnetic wave propagation velocity at low radio frequencies is a critical parameter for time-of-arrival (TOA) based lightning location systems and thus directly affects the feasibility of global lightning mapping with VLF sferics [22]. Therefore, phase coherency analysis enhances location accuracy compared to traditional time of arrival methods and enables a more reliable worldwide monitoring of lightning activity. This represents a significant step toward comprehensive global lightning observation systems and enables global lightning monitoring networks, which are critical for studying storm dynamics, climate impacts, and space weather coupling. Lightning sferics can serve as natural probes of electron density variability and highlight the potential of coherency methods to contribute to space weather monitoring, bridging atmospheric science with geophysical applications. Phase coherency approaches using Hilbert transforms to derive analytic signals demonstrate that coherency waveforms reveal distance dependent impulse responses and improve lightning location accuracy compared to amplitude-based methods [23]. Coherency methods can mitigate skywave interference in long-range lightning detection and pave the way for global lightning mapping systems [24]. Collectively, these studies demonstrate that coherency analysis of lightning sferics provides a powerful framework for both lightning mapping and ionospheric diagnostics. While traditional amplitude-based methods remain useful, phase-based coherency approaches offer improved accuracy, robustness against skywave interference, and expanded applications in atmospheric and space science. The field is moving toward integrating coherency into global monitoring networks, with implications for climate studies, storm dynamics, and space weather forecasting.

The coherency of lightning sferics, the broadband radio pulses emitted by lightning, has been studied to improve detection methods. Traditionally, lightning detection networks rely on time of arrival differences to triangulate strike locations. A coherency based interferometric approach was introduced, analyzing the phase stability of lightning signals using tools such as the Hilbert transform. By examining coherency, it was shown that lightning can be mapped into a two-dimensional area of pixels, each with different coherency values, rather than just a single point. This method improves accuracy and provides richer information about lightning sources. [23]. This work tries to explain how and why lightning sferics acquire their coherence. The key parallel to twisted (helical wavefront bremsstrahlung radiation) electromagnetic wave is that coherence preserves structure: in emitted bremsstrahlung radiation, the helical wavefront means emitted radiation has coherency; hence, in lightning, it stabilizes the radio signal's phase, enabling precise mapping.

2 Aims & Objectives

This report investigates the rotational tendency of the wavefront of a wave emitted by bremsstrahlung process using curl of a gradient of the radiation intensity field and Huygen's principle.

3 Understanding Rotating Wavefront in Bremsstrahlung Radiation

As mentioned bremsstrahlung photons can have not just spin angular momentum (polarisation), but also orbital angular momentum. When photons carry orbital angular momentum, their wavefronts twist like a corkscrew, giving the radiation a helical structure. This means source, which is the bremsstrahlung particle has a rotational or magnetic symmetry. A helical photon trajectory usually originates from a source with rotational motion or source with magnetic fields. As it is known, bremsstrahlung electrons in the atmosphere, travel under Earth's magnetic field hence, they follow a helical path. Another example to this is synchrotron radiation (electrons spiralling in magnetic fields).

A helical path implies coherence and structure in the emission. Helical photons can transfer angular momentum to matter. This means the source is not emitting energy, but also rotational momentum, revealing the dynamics of the emitting system. Helical photon path often indicates a charged particle spiraling in magnetic fields, which is the case with a bremsstrahlung electron travelling in Earth's magnetic field.

Normal light (polarisation) only has two states. However, light consisting of helical photons has many possible states, for example ($l = ... - 3, -2, -1, 0, +1, +2, +3...$). Each l angular momentum value corresponds to a different helical wavefront. As discovered, bremsstrahlung asymmetry can affect the radiation intensity, hence frequency and phase of the helical wavefront. This introduces different helical wave modes and multiple possible angular momentum states.

4 Curl of Doppler and Bremsstrahlung Asymmetric Radiation Pattern

In a previous analysis of Bremsstrahlung asymmetry under periodic radiation emission, the Bremsstrahlung radiation pattern with all the asymmetries was simplified into [25]

$$\frac{d^2I}{d\omega\Omega_{rad}} = \left| sin(\theta_{n,\beta}) e^{-\frac{y^2\alpha^{-2}}{8}} \right|^2, \tag{1}$$

Where, α is $\alpha^2 = \frac{b^R(\gamma\omega(S_{SpecialR} - \beta S_{SpecialR} cos(\theta_{n,\beta})))^R (sin(\theta_{n,\beta}))^R}{(\tau^R)^2 c^R}$ $[s^{-2}]$, and y is $y = \frac{\gamma\omega(S_{SpecialR} - \beta S_{SpecialR} cos(\theta_{n,\beta})) sin(\theta_{n,\beta}) a}{c\tau}$ $[\mathrm{s}^{-1}]$.

Equation 1 is the simplified version of main bremsstrahlung asymmetric radiation pattern equation. It still contains all the physical information of bremsstrahlung asymmetry, Doppler effect, and preserves peaking radiation pattern.

By taking the Curl of the gradient of equation 1, rotational mode of the bremsstrahlung asymmetric radiation pattern can be modelled and predicted.

$$\boldsymbol{\nabla} \times \nabla \frac{d^2I}{d\omega\Omega_{rad}} \neq 0$$

Parameters inside equation 1 that are constant in each bremsstrahlung interaction

$$C_1 = \frac{b^R}{(\tau^R)^2 c^R}$$

and constant two

$$C_2 = \frac{a\gamma S_{SpecialR}}{c\tau}$$

Hence, equation 1 simplifies to Equation 2

$$\frac{d^2I}{d\omega\Omega_{rad}} = \left| sin(\theta_{n,\beta}) e^{-\frac{\left[C_2(\omega - \beta\omega cos(\theta_{n,\beta})) sin(\theta_{n,\beta})\right]^2}{8\left[C_1(\gamma\omega(S_{SpecialR} - \beta S_{SpecialR} cos(\theta_{n,\beta})))^R (sin(\theta_{n,\beta}))^R\right]^2}} \right|^2 \tag{2}$$

Since radiation intensity is a scalar field, the curl operator cannot be applied directly to a scalar. Hence, first the gradient of a scalar is found and then the curl of that gradient is calculated.

Curl in Polar co-ordinates $r(\omega, \beta, \theta_{n,\beta}) = \frac{d^2I}{d\omega\Omega_{rad}}(\omega, \beta, \theta_{n,\beta})$ can be calculated using,

$$\boldsymbol{\nabla} \times \nabla \frac{d^2I}{d\omega\Omega_{rad}} = \frac{1}{r}\frac{\delta}{\delta\omega}\left(r\left[\nabla \frac{d^2I}{d\omega\Omega_{rad}}\right]_{\theta_{n,\beta}}\right) - \frac{1}{r}\frac{\delta}{\delta\theta_{n,\beta}}\left[\nabla \frac{d^2I}{d\omega\Omega_{rad}}\right]_r \tag{3}$$

In polar coordinates the formula for gradient is:

$$\nabla \frac{d^2I}{d\omega\Omega_{rad}} = \hat{r}\frac{\delta}{\delta\omega}\frac{d^2I}{d\omega\Omega_{rad}} + \hat{\theta}\frac{1}{r}\frac{\delta}{\delta\theta}\frac{d^2I}{d\omega\Omega_{rad}} \tag{4}$$

Hence,

$$\nabla \frac{d^2I}{d\omega\Omega_{rad}} = \hat{r}\frac{K^2(-1+R)\omega(-1+\beta\cos(\theta))^2 \sin^{4-2R}(\theta)\Re'\left(\frac{K^2(\omega-\beta\omega\cos(\theta))^2\sin^{2-2R}(\theta)}{(L\gamma\omega(S-S\beta\cos(\theta)))^{2R}}\right)}{2e^{\left(\frac{1}{4}\Re\left(\frac{K^2(\omega-\beta\omega\cos(\theta))^2\sin^{2-2R}(\theta)}{(L\gamma\omega(S-S\beta\cos(\theta)))^{2R}}\right)\right)}(L\gamma\omega(S-S\beta\cos(\theta)))^{2R}} + \hat{\theta_{n,\beta}}\frac{1}{\left|sin(\theta_{n,\beta})e^{-\frac{y^2\alpha^{-2}}{8}}\right|^2} \frac{\sin(\theta)\left(8\cos(\theta) - \frac{2K^2(-1+R)\omega^2(-1+\beta\cos(\theta))\sin^{2-2R}(\theta)\left(\cos(\theta)-\beta\cos^2(\theta)+\beta\sin^2(\theta)\right)\Re'\left(\frac{K^2(\omega-\beta\omega\cos(\theta))^2\sin^{2-2R}(\theta)}{(L\gamma\omega(S-S\beta\cos(\theta)))^{2R}}\right)}{(L\gamma\omega(S-S\beta\cos(\theta)))^{2R}}\right)}{4e^{\left(\frac{1}{4}\Re\left(\frac{K^2(\omega-\beta\omega\cos(\theta))^2\sin^{2-2R}(\theta)}{(L\gamma\omega(S-S\beta\cos(\theta)))^{2R}}\right)\right)}} \tag{5}$$

Equation 5 describes the gradient of the scalar radiation intensity field. Equation 5 allows us to calculate the curl of the emitted radiation pattern described in equation 2.

Equation 5 shows that the curl of a gradient of radiation intensity field is non-zero because the equation involves non smooth functions such as reciprocal function $(1/r)$, modulus function $(|r|)$,

and multivalued functions like angle $\theta_{n,\beta}$. Therefore, indicating that the radiation pattern could possess a rotating helical wavefront. From a physics perspective, asymmetry inside the bremsstrahlung radiation intensity is the cause of the curl of a gradient of radiation intensity field being non zero. Bremsstrahlung asymmetry, defined with quantity R, measures the asymmetry in radiation intensity between lobes due to particle's curved trajectory. Quantity R has discrete values and similar to standing electron wave, it can only take certain values. One bremsstrahlung asymmetry "R" value accounts for certain range of radius of curvatures a particle can follow.

Figure 1 is the curl plot of the radiation intensity field gradient describing the rotational tendency of the radiation wavefront. The Curl was found to be non-zero, supporting the idea of a bremsstrahlung wavefront following a helical pattern.

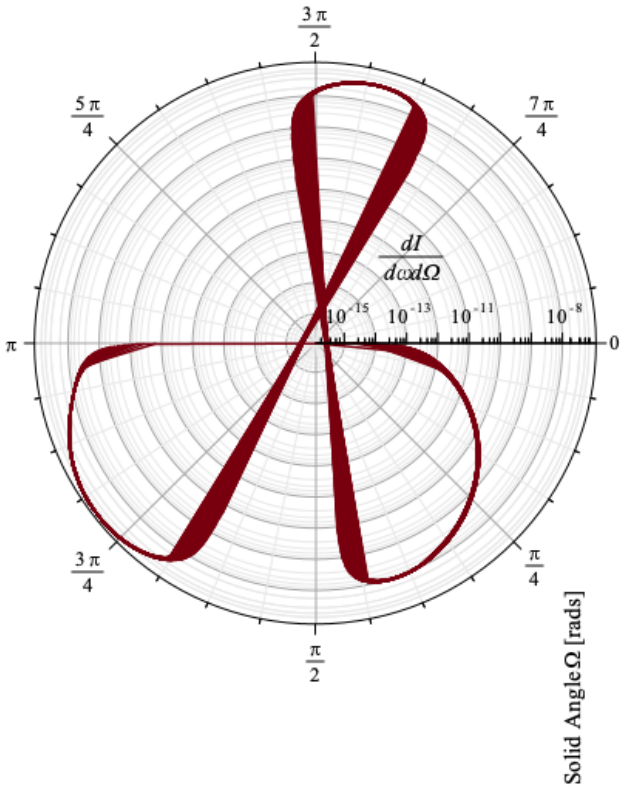

Figure 1. Plot of the curl of the gradient of scalar radiation intensity field around a single particle undergoing a bremsstrahlung process. Plot of equation 3. The angle in this figure is the Azimuthal angle around the particle. Bremsstrahlung and Doppler Asymmetries causing difference in the radius of the rotation (circulation) of the energy flow from the wave. This is causing spatial coherence to disappear.

The rotational property of the bremsstrahlung wavefront is also explained using Huygen's principle. As can be seen in Figure 2, the resulting wavefront follows a 2D spiral, which in 3D can form a helical path.

Rotational wavefront hides the direct observation of bremsstrahlung asymmetry and four peaking radiation lobes by turning the wave into spiral and helical emission patterns as described using Huygen's principle and by taking the curl of the gradient of the radiation intensity field.

Moreover, this indicates that even if the radiation pattern of a single bremsstrahlung particle were to be measured, the four peaking radiation lobes, including the bremsstrahlung and Doppler asymmetries [26], would all have been hidden under the resultant spiral and helical wavefront radiation pattern. In addition, the clue for the presence of four peaking radiation lobes with the bremsstrahlung and Doppler asymmetries could be found in the asymmetry of the radius of curvature of the twisted helical and spiral wavefront about the axis of direction of motion of a particle. The asymmetric spiral radius is displayed on the curl plot in figure 4 and figure 5. Figure 4 shows the temporal evolution of the rotating phase of the bremsstrahlung radiation. Every time frame captures the full rotation and displays how full rotation evolves in time. Figure 5 shows how single full rotation is achieved.

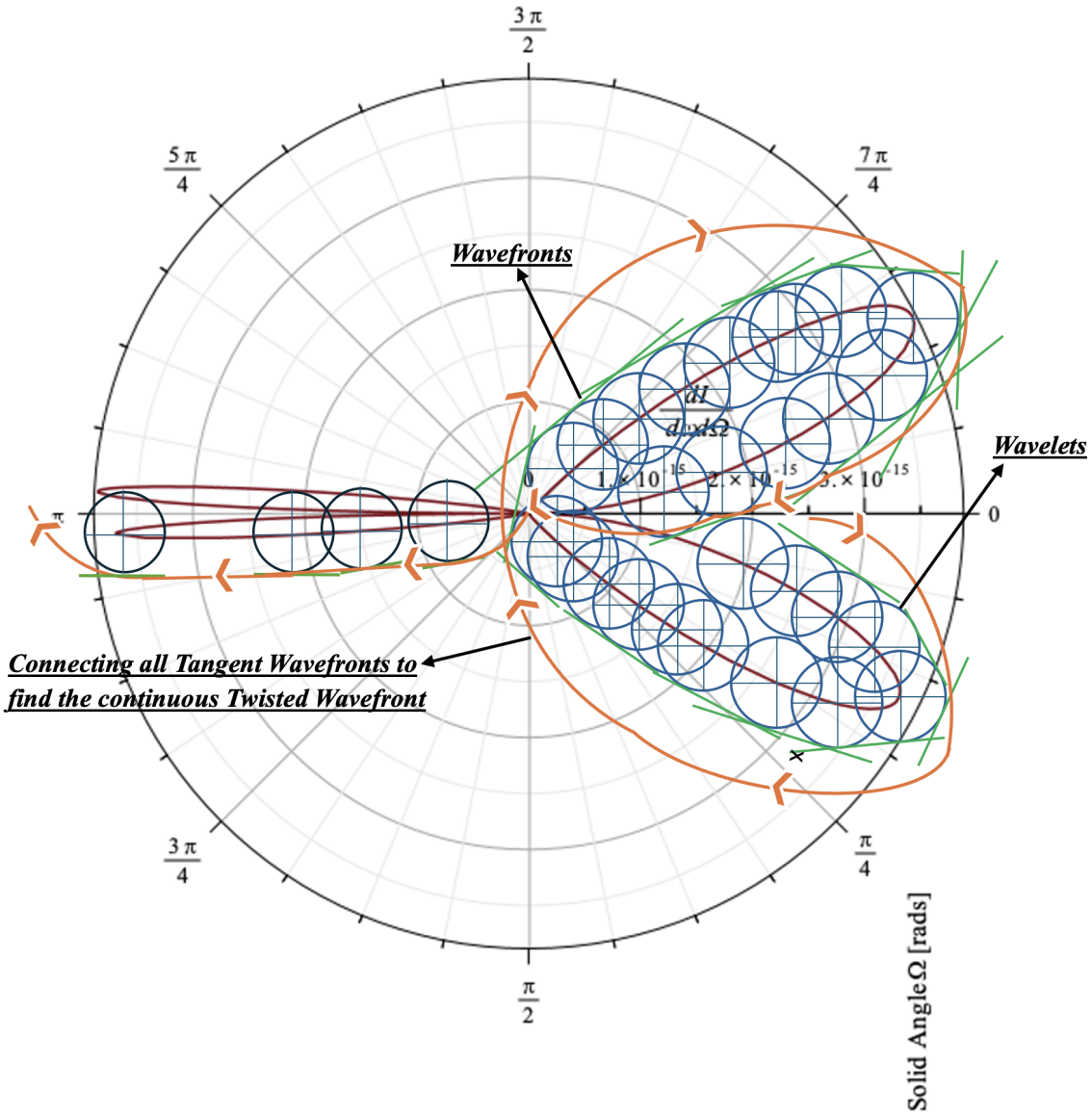

Figure 2. Huygens' principle states that every point on a wavefront acts as a source of secondary spherical wavelets, and the new wavefront at a later time is the surface tangent to all these wavelets. As can be seen, by applying Huygens' principle to the bremsstrahlung asymmetric forward-backward peaking radiation pattern, the wavefront was found to be propagating in twisted wavefront form.

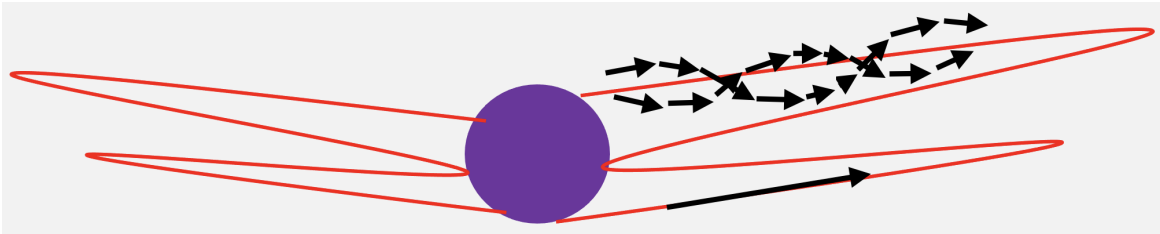

Figure 3. The rotation of the bremsstrahlung photons following helical path inside the radiation pattern around the axis of direction of motion of the wave. Rotating helical black arrows are the 3 dimensionally connected green lines in Figure 2 showing the continuously connected version of secondary spherical wavelets.

Curl of the gradient of scalar radiation intensity field produces a nonzero azimuthal curl (curl in "r" and $\theta_{n,\beta}$ plane gives a vector perpendicular to this plane which is in the azimuthal direction) which means there is local circulation of energy, but it is not by itself a proof that phase surfaces (wavefronts) are rotating in time. It is a strong indicator of circulating energy or orbital angular momentum, yet the rotation of wavefronts requires explicit time evolution of the phase.

Hence, the curl of the gradient of the scalar radiation intensity field is observed with different input time values, and the wavefront was found to be rotating around the particle in time, similar to the initial prediction with Huygen's principle, matching the predictions of the curl plot. Spiral rotation was found to be moving in a backward direction with decreasing radius of rotation. Afterwards, the radius disappears, and the rotating wavefront turns into Dipole radiation. This can be seen in Figure 4.

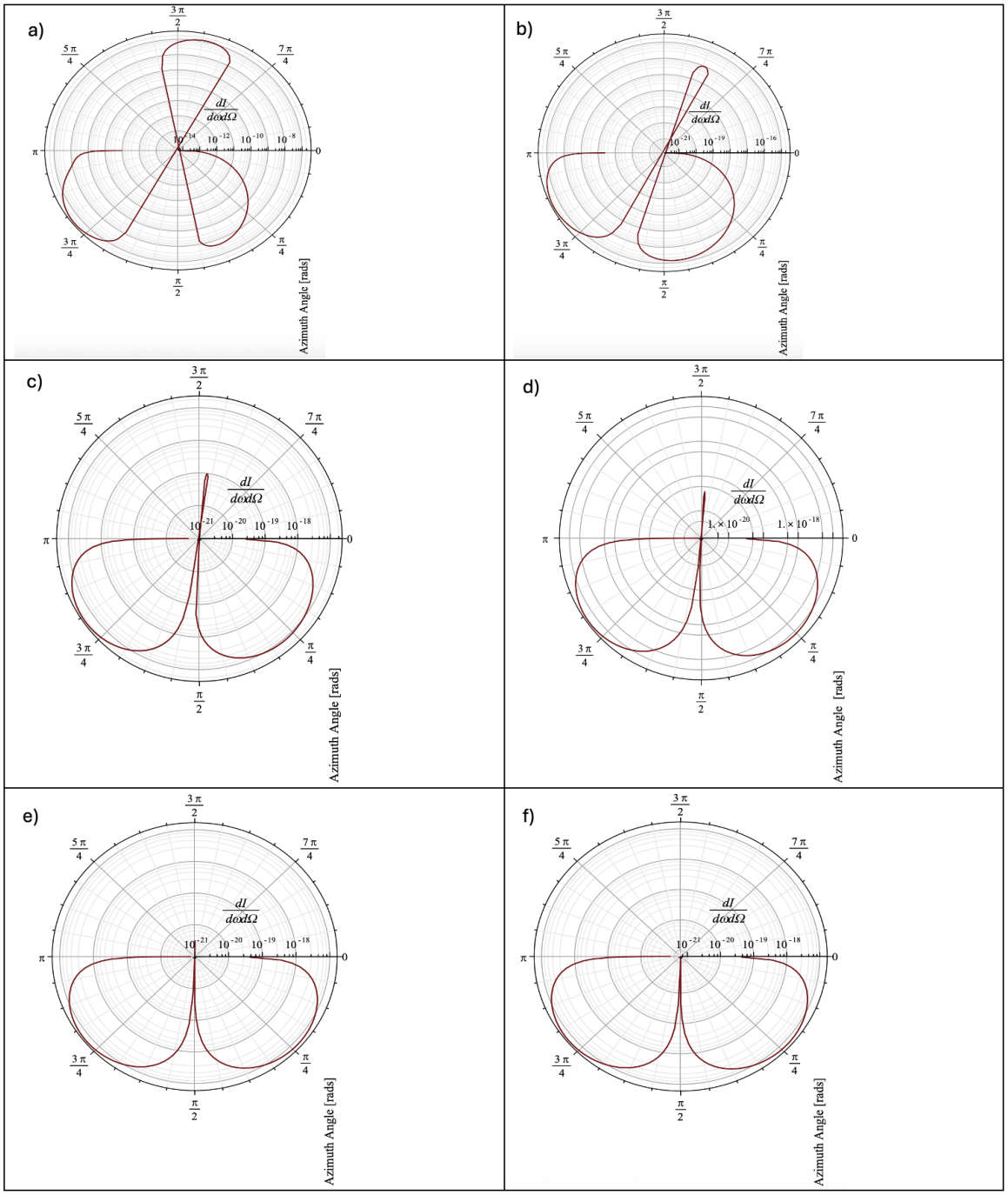

Figure 4. Display of temporal evolution of the rotating phase of the bremsstrahlung radiation. Every time frame captures the full rotation and displays how full rotation evolves in time. Order of magnitude of time, "t" from a to f is: $t_f > t_e > t_d > t_c > t_b > t_a$

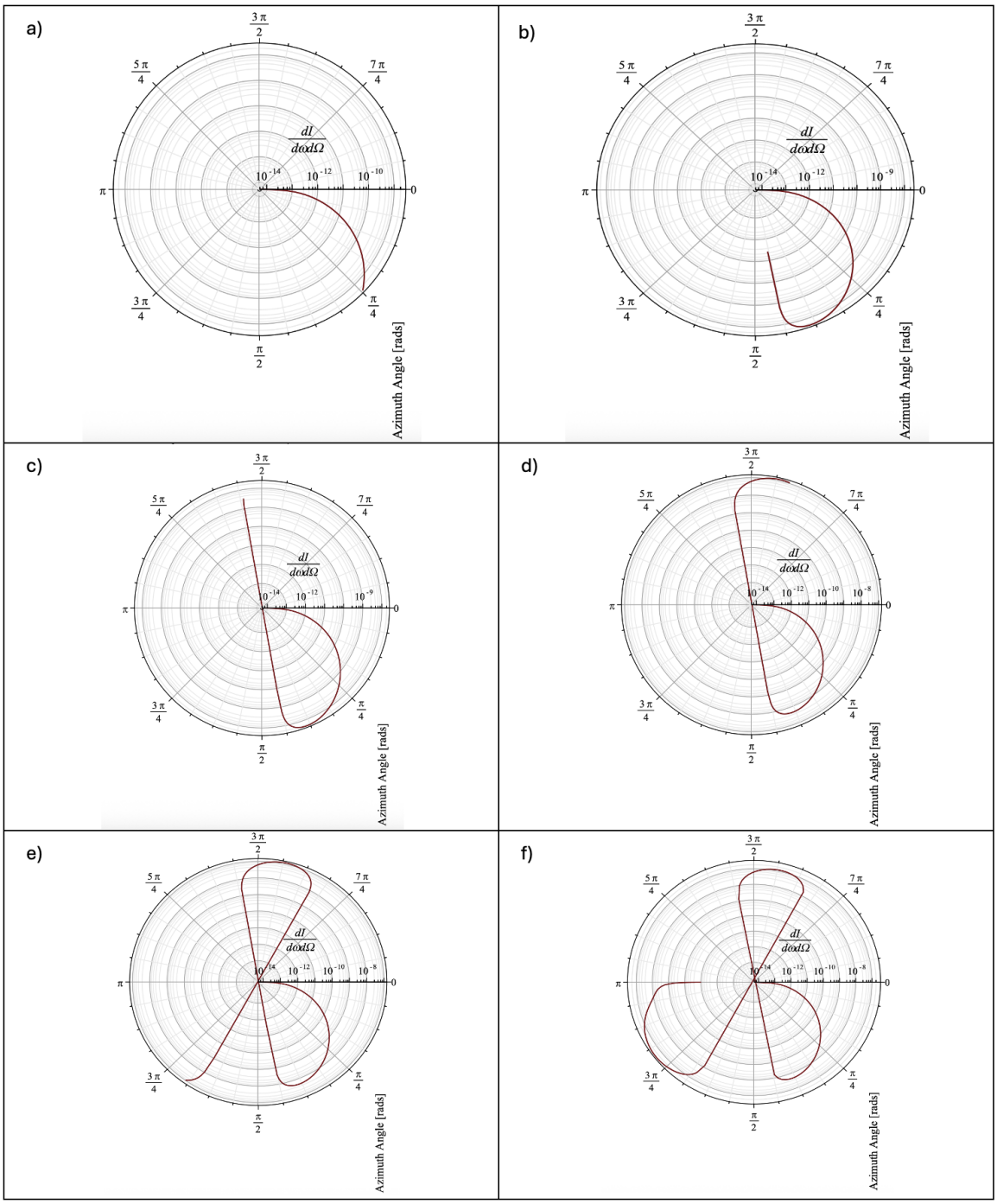

Figure 5. Demonstration of single full phase rotation of high energy forward-backward peaking radiation pattern during the initial phase of its rotation.

Figure 5 shows the azimuthal angular rotation direction of the backward moving tapered spiral radiation wavefront.

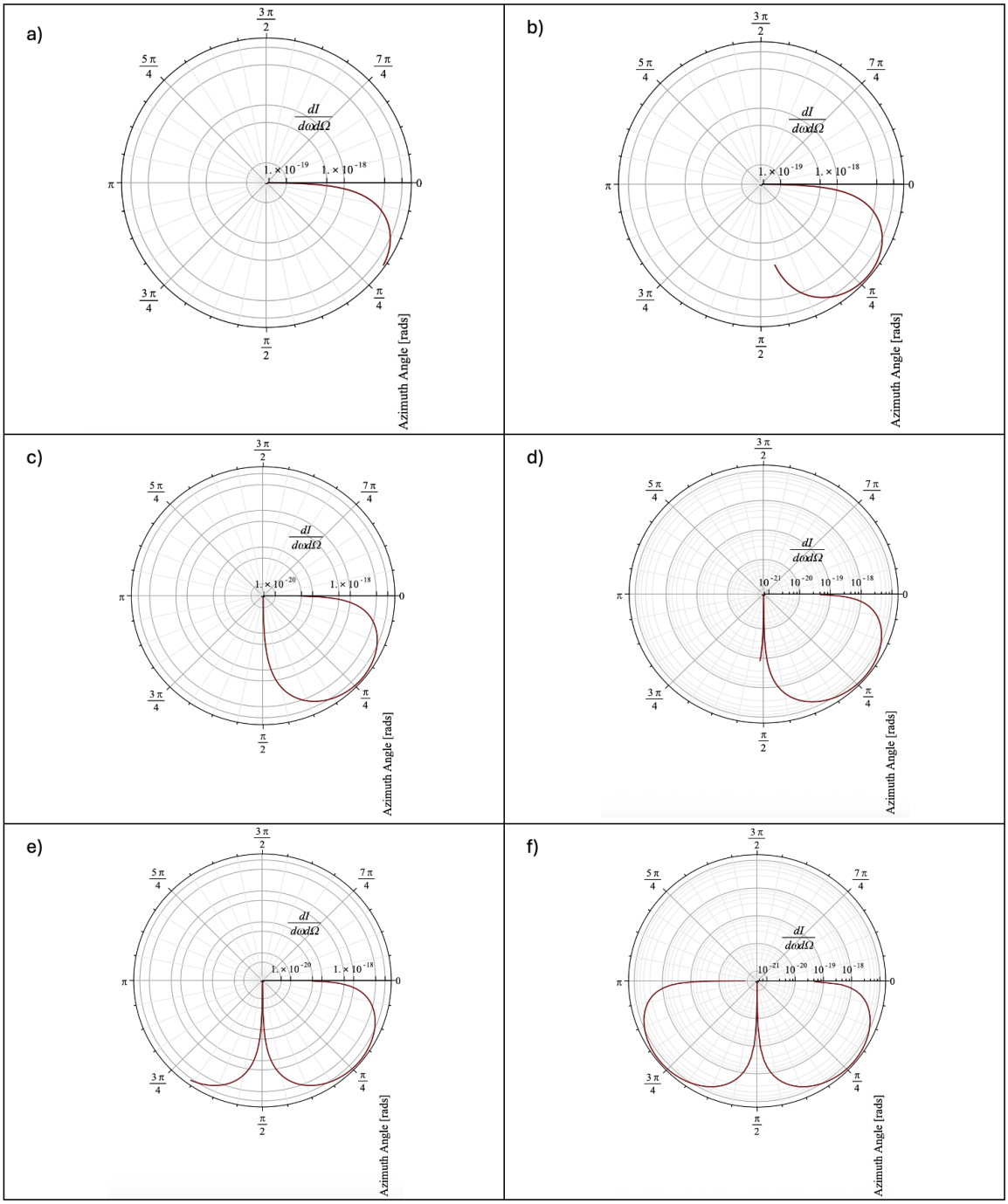

Figure 6. Demonstration of single full phase rotation of high energy forward-backward peaking radiation pattern in the final stages of its phase rotation.

Figure 6 shows the azimuthal angular rotation direction of the dipole radiation wavefront as the final stage of the initial backward moving tapered spiral wavefront.

5 Action of Physics

Aim of this section is to understand why Bremsstrahlung asymmetry,R exists and why it is limited to only certain discrete values between, 1/9 and 1/3.

In sequence, from the work of Pierre Louis Maupertuis on the principle of least action, $S = \int mvds$, Joseph-Louis Lagrange on the principle of Lagrangian define as the difference between the kinetic energy (T) and the potential energy (V) of a system $L = T - V$, Hamilton's principle of Least Action defining action as time integral of Lagrangian, $S = \int (T - V)dt$, the Rayleigh-Jeans Law describing the spectral radiance of blackbody radiation at long wavelengths $I_\lambda(T) = \frac{2ck_BT}{\lambda^4}$ using a metal cube that allows radiation to get inside and the walls of the cube wiggling around producing standing waves with discrete modes (n). Finally, Planck's work on short wavelengths of Black-body radiation, which led to Quantum of Action "S" given by equation 6:

$$S = nh \tag{6}$$

We know from Bohr's work that angular momentum $L = mvr$ has the same unit as the units of the Action, hence they can be equated to each other and equation 6 can be re-written as equation 7:

$$nh = mvr \tag{7}$$

Momentum transfer from particle to rotating wavefront photon, quantized via conservation of momentum, $p_f - p_i = -\Delta P_{field}$, and $\Delta P_{field} = (n' - n)\,\hbar k = \Delta n\,\hbar k$. Therefore, $p_f = p_i - \Delta n\,\hbar k$ where p_i, and p_f are initial and final particle momentum. Hence, the relationship between bremsstrahlung asymmetry, R, as a function of the whole number multiple of the quantum of action "n", R(n), is

$$nh = mv\left[\frac{(t^R)^2 b^R (\omega')^R cos(\theta_{n,r(t)})^R c}{\tau^{2R} c^R \omega' cos(\theta_{n,r(t)})} - \frac{at}{\tau}\right] \tag{8}$$

Position vector $r(t)$ comes from a paper describing bremsstrahlung asymmetry "Asymmetric Backward Peaking Radiation Pattern From a Relativistic Particle Accelerated by Lightning Leader Tip Electric Field" [26][p. 5, Eq. 1].

Re-arranging equation 8 to make "R" subject of the formula:

$$R = \frac{ln\Big(-\frac{\omega'\left(-\frac{at}{\tau} - \frac{nh}{mv}\right)}{c}\Big) + ln(cos(\theta_{n,r(t)}))}{ln(b) - ln(c) + ln(cos(\theta_{n,r(t)})) + 2ln(t) - 2ln(\tau) + ln(\omega')} \tag{9}$$

Equation 9 is the discretised, quantum bremsstrahlung asymmetry. This will tell us how "R" progresses and what is the earliest minimum asymmetry that starts within the electron that leads to the asymmetric radiation emission.

Following from the publication [26, p. 15], to ensure that the Bremsstrahlung radiation patterns are plotted from the velocity vector, around the particle, the relationships of $sin(\theta_{n,\beta}) = \frac{r(t)}{n}$ and $cos(\theta_{n,r(t)}) = \frac{r(t)}{n}$ are used to relate two angles together $sin(\theta_{n,\beta}) = cos(\theta_{n,r(t)})$. Changing the angle of observation by substituting $sin(\theta_{n,\beta}) = cos(\theta_{n,r(t)})$ into the equation 9 gives:

$$R = \frac{ln\Big(-\frac{\omega'\left(-\frac{at}{\tau} - \frac{nh}{mv}\right)}{c}\Big) + ln(sin(\theta_{n,\beta}))}{ln(b) - ln(c) + ln(sin(\theta_{n,\beta})) + 2ln(t) - 2ln(\tau) + ln(\omega')} \tag{10}$$

As can be seen in Figure 8, pattern 1 is the plot of equation 10. That form represents the first multiple of Planck's constant "nh". It also shows Bremsstrahlung asymmetry exceeding 1/8. Bremsstrahlung asymmetry, R in equation 10, should represent Figure 7. If we re-scale the figure 8, pattern 1 plot to the correct bremsstrahlung asymmetry using the only remaining variable, which is the multiples of Planck's constant "n", we get a new plot as Figure 8, pattern 4. We can see that there is no asymmetry on the top of the particle, above the horizontal axis, which is the correct representation. We can also see that asymmetry in radiation disappears towards the particle at the origin and is maximum at the forward and backward peaking ends. Furthermore, since bremsstrahlung asymmetry R scales properly using the only remaining variable, which is the multiples of Planck's constant "n", in terms of quantized momentum of a photon, only Orbital angular momentum, $n\hbar$ per photon, scales with multiples of Planck's constant "n". This means the photons of the bremsstrahlung radiation must be following helical path as they move in the direction of the forward-backward peaking radiation pattern. (helical wavefront modes).

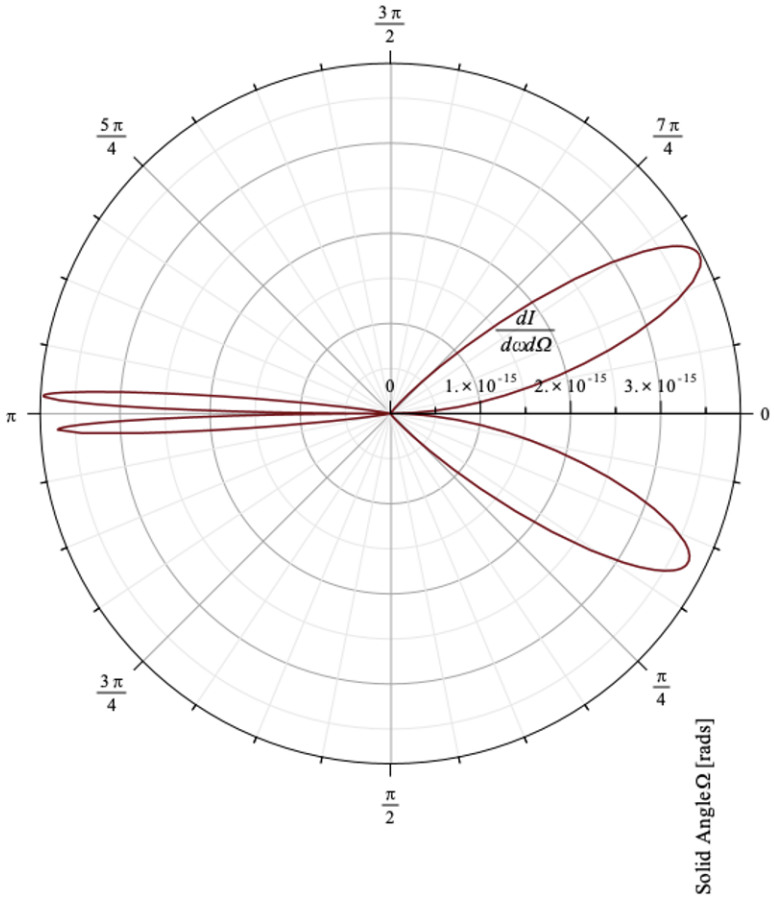

Figure 7. Simulated high energy particle properties: $t = 1.62 \times 10^{-9}s$, emitted radiation frequency, $f_{Rs} : 100MHz$, mean free time, $\tau = 30 \times 10^{-6}$, $a = 100 \times 10^{-6}$, $b = 10^{-9}$, $s_f = 1$, $s_{ft} = 1$, $z = 1$, $s_{fv} = 8.19 \times 10^{-11}$, Bremsstrahlung Asymmetry, $R = \frac{1}{8}$

Table 1. *Bohr's Correspondence Principle via Bremsstrahlung Asymmetry, R:* Quantum of Action is Planck's Constant, h and we multiply it with whole number multiples, n to get multiples of quantum of action nh for Correspondence Principle. As multiple of quantum of action increases to a certain value, bremsstrahlung asymmetry, R plot starts to represent the bremsstrahlung asymmetry observed in the radiation intensity graph displayed in Figure 7. Patterns 4 and 5 are the matching patterns describing the bremsstrahlung asymmetry, in Figure 8 which was set to $\frac{1}{8}$.

Bremsstrahlung Asymmetry, R Patterns	Whole number Multiples of Quantum of Action, n
Pattern 1	1
Pattern 2	6×10^6
Pattern 3	6×10^9
Pattern 4	6×10^{10}
Pattern 5	6.3×10^{10}
Pattern 6	6.7×10^{10}

The Bohr correspondence principle tells us that quantum mechanics and classical physics must agree in the limit of very large quantum numbers. In other words, when the quantum number "n" becomes very large, the discrete (quantised) behaviour predicted by quantum mechanics should start to look like the smooth, continuous behaviour described by classical physics.

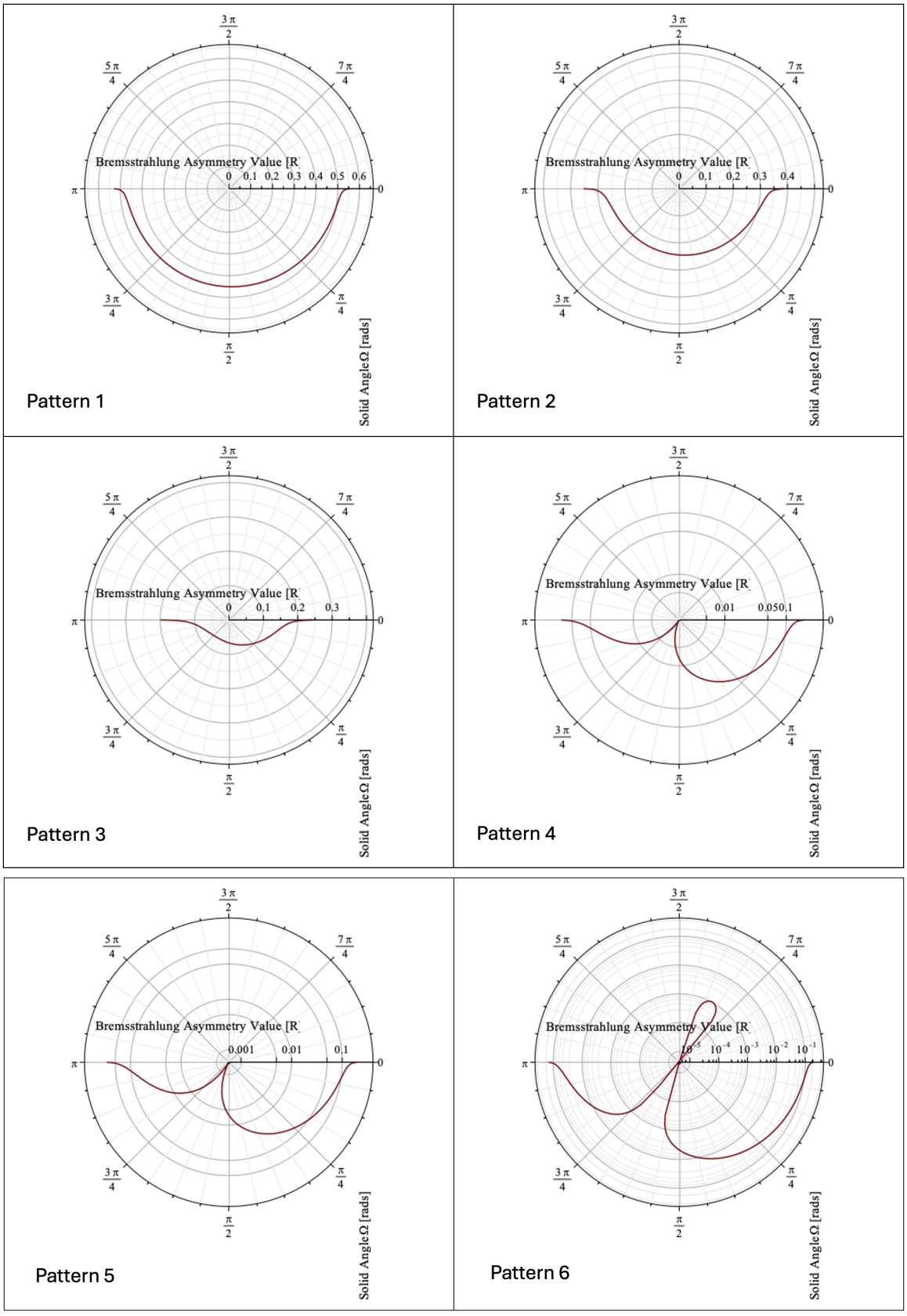

Figure 8. As can be seen, pattern 4 and 5 are achieved following the Bohr correspondence principle which tells us that quantum mechanics and classical physics must agree in the limit of very large quantum numbers. Hence, by increasing the quantum multiples of quantum of Action, "n" to $n \approx 6.3 \times 10^{10}$ we can start to see that the new form of graph which describes the bremsstrahlung asymmetry quantity, R goes from pattern 1 to pattern 5 and starts to match and describe exactly the results observed in the classical predictions of the bremsstrahlung asymmetry, R in the emitted radiation patterns of a single bremsstrahlung particle shown in Figure 7.

6 Even Denominator Bremsstrahlung Asymmetry, R Value for Rotational Wavefront Modelling

Using the clue and information of how bremsstrahlung asymmetry, R contributes to rotational wavefront from Huygen's principle analysis. This section use even number denominator forms of Bremsstrahlung asymmetry R, to re-write equation 1 as a complex number involving phase for wavefront analysis.

Using the variable $\alpha^2 = \frac{b^R(\gamma\omega(S_{SpecialR} - \beta S_{SpecialR} cos(\theta_{n,\beta})))^R (sin(\theta_{n,\beta}))^R}{(\tau^R)^2 c^R}$ $[s^{-2}]$ in equation 1. Quantity $(sin(\theta_{n,\beta}))^R$ inside α for any even number denominator of the Bremsstrahlung asymmetry, R, we can decompose the fraction as the square root multiplied by the remaining fraction for the full fraction of the Bremsstrahlung asymmetry.

To understand what happens to the quantity $sin(\theta_{n,\beta})^R$ when denominator of "R" is an even number, such as $R = \frac{1}{8}$. The quantity $sin(\theta_{n,\beta})^R$ becomes $sin(\theta_{n,\beta})^{\frac{1}{8}} = (sin(\theta_{n,\beta})^{\frac{1}{2}})^{\frac{1}{4}} = (\sqrt{sin(\theta_{n,\beta})})^{\frac{1}{4}}$. Therefore, for when $\sin(\theta_{n,\beta}) < 0$,

Expression

$$\sqrt{sin(\theta_{n,\beta})}$$

, taking the square root of a negative number requires complex numbers. Considering the simplest case:

$$-1$$

.

Using Euler's formula,

$$-1 = e^{i\pi},$$

since

$$e^{i\pi} = \cos(\pi) + i\sin(\pi) = -1.$$

Expressing a negative sine in exponential form for when $\sin(\theta_{n,\beta}) < 0$, then

$$sin(\theta_{n,\beta}) = -|sin(\theta_{n,\beta})|.$$

As

$$-1 = e^{i\pi}.$$

. Thus, the negative sine can be re-written as

$$sin(\theta_{n,\beta}) = |sin(\theta_{n,\beta})|\, e^{i\pi}.$$

Therefore, Polar decomposition of $sin(\theta_{n,\beta})$ and bremsstrahlung asymmetry R can be written as:

Let $(\theta_{n,\beta})$ be written in polar form as

$$\sin\theta_{n,\beta} = r\, e^{i\varphi}, \tag{11}$$

where

$$r = |\sin\theta_{n,\beta}|, \qquad \varphi = phase$$

The reason for why only the quantity $(sin(\theta_{n,\beta}))^R$ inside α is written in the form $r\, e^{i\varphi}$ is that it is the only parameter when the denominator of R is an even number, the fraction value of "R" can be separated to form taking square root of a negative number leading to the imaginary phase term of the radiation. There are no any other parameter with an index "R" that can produce taking square root of a negative number leading to imaginary phase term. Identifying this is the crucial and most important step in transforming the radiation intensity patterns to include phase information of the emitted wave.

The principal square root of $\sin\theta_{n,\beta}$ is then

$$\sqrt{\sin\theta} = \sqrt{r}\, e^{i\varphi/2},$$

where $\sqrt{r}$ denotes the nonnegative real square root of r.

Therefore, for any even number denominator of the Bremsstrahlung asymmetry, R we can write,

$$(sin(\theta_{n,\beta}))^R = \left(\sqrt{|\sin\theta_{n,\beta}|}\, e^{i\varphi/2}\right)^{2R} \tag{12}$$

Equation 12 can be simplified to,

$$(sin(\theta_{n,\beta}))^R = (|\sin\theta_{n,\beta}|)^R\, e^{iR\varphi} \tag{13}$$

Equation 13 is a novel approach and extended form of novel forward-backward peaking, asymmetric radiation intensity patterns to include phase rotation for wavefront modeling.

Substituting equation 13 into variable α replacing quantity $(sin(\theta_{n,\beta}))^R$ gives,

$$\alpha^2 = \frac{b^R(\gamma\omega(S_{SpecialR} - \beta S_{SpecialR} cos(\theta_{n,\beta})))^R \left((|\sin\theta_{n,\beta}|)^R\, e^{iR\varphi} \right)}{(\tau^R)^2 c^R} \tag{14}$$

Equation 14 along with equation 1 describes both intensity and phase for wavefront motion of the emitted bremsstrahlung wave.

Full equation can be written as,

$$\frac{d^2I}{d\omega\Omega_{rad}} = \left| sin(\theta_{n,\beta}) e^{-\frac{y^2(\tau^R)^2 c^R}{8b^R(\gamma\omega(S_{SpecialR} - \beta S_{SpecialR} cos(\theta_{n,\beta})))^R \left((|\sin\theta_{n,\beta}|)^R, e^{iR\varphi} \right)}} \right|^2, \tag{15}$$

For convenience let's assume new form of alpha is capital Greek letter Upsilon $\Upsilon = \frac{(\tau^R)^2 c^R}{8b^R(\gamma\omega(S_{SpecialR} - \beta S_{SpecialR} cos(\theta_{n,\beta})))^R (|\sin\theta_{n,\beta}|)^R}$

Therefore, we can re-write equation 15 as,

$$\frac{d^2I}{d\omega\Omega_{rad}} = \left| sin(\theta_{n,\beta}) e^{-\frac{y^2\Upsilon}{e^{iR\varphi}}} \right|^2 \tag{16}$$

Using the identity

$$\frac{1}{e^{iR\varphi}} = e^{-iR\varphi},$$

the exponent becomes

$$\frac{d^2I}{d\omega\Omega_{rad}} = \left| sin(\theta_{n,\beta}) e^{-y^2\Upsilon(e^{-iR\varphi})} \right|^2 \tag{17}$$

Expanding the complex exponential using Euler's formula which is

$$e^{-iR\varphi} = \cos(R\varphi) - i\sin(R\varphi)$$

gives,

$$\frac{d^2I}{d\omega\Omega_{rad}} = \left| sin(\theta_{n,\beta}) e^{-y^2\Upsilon(\cos(R\varphi) - i\sin(R\varphi))} \right|^2 \tag{18}$$

Therefore the field separates into amplitude and phase:

$$\frac{d^2I}{d\omega\Omega_{rad}}(\theta_{n,\beta},\varphi) = \left| sin(\theta_{n,\beta}) e^{-y^2\Upsilon\cos(R\varphi)} e^{iy^2\Upsilon\sin(R\varphi)} \right|^2 \tag{19}$$

Inside equation 19, the first exponential is real amplitude and the second exponential is pure phase of the emitted forward-backward peaking bremsstrahlung radiation pattern.

To simulate and observe the wavefront pattern, only the second imaginary exponential describing phase Φ part of the equation 19 is needed.

Hence, phase of the complex radiation field can be written as,

$$\Phi(\theta_{n,\beta},\varphi) = y^2\Upsilon\sin(R\varphi) \tag{20}$$

The phase is the argument of the imaginary exponential as given in equation 20.

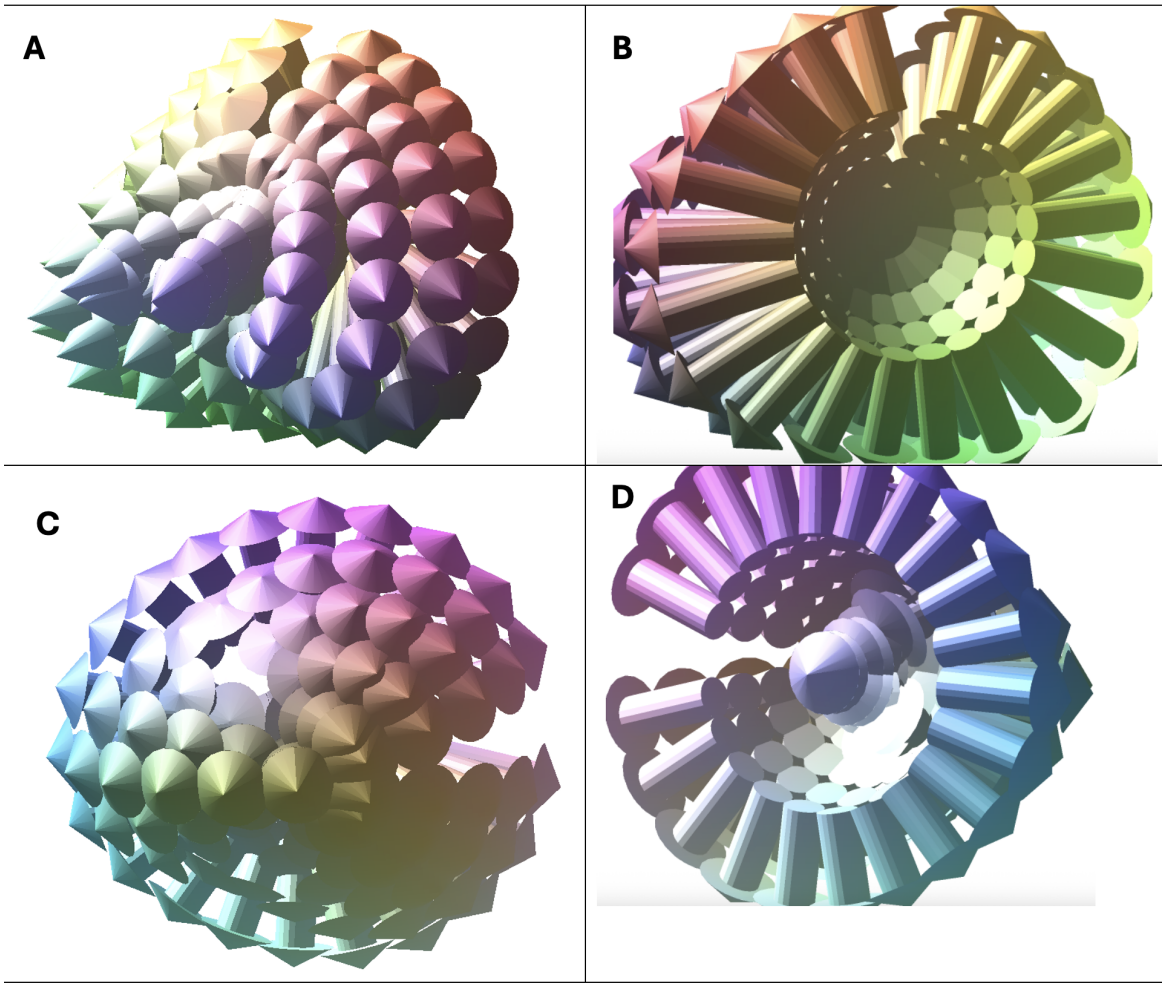

Figure 9. Figure 9 is the 3D phase plot of the emitted forward-backward peaking bremsstrahlung radiation with non-normalised vector length. Radiation phase is demonstrated on 3D spherical surface. Figure 9A is the top half of the spherical surface. Figure 9B is inside of the top half of the sphere. Figure 9C is the bottom half of the spherical surface. Figure 9D is inside of the bottom half. As known from Figure 5 and Figure 8, spiral rotation starts at the front direction and rotation moves to the backward direction. Figure 5C-E exactly shows that transition of rotation from forward to backward directions.

3D model successfully predicts and matches with the previous prediction of the spiral rotation of the bremsstrahlung wavefront. As known from Figure 5 and Figure 8, spiral rotation starts at the front direction and rotation moves to the backward direction. Figure 5C-E exactly shows that transition of rotation from forward to backward directions.

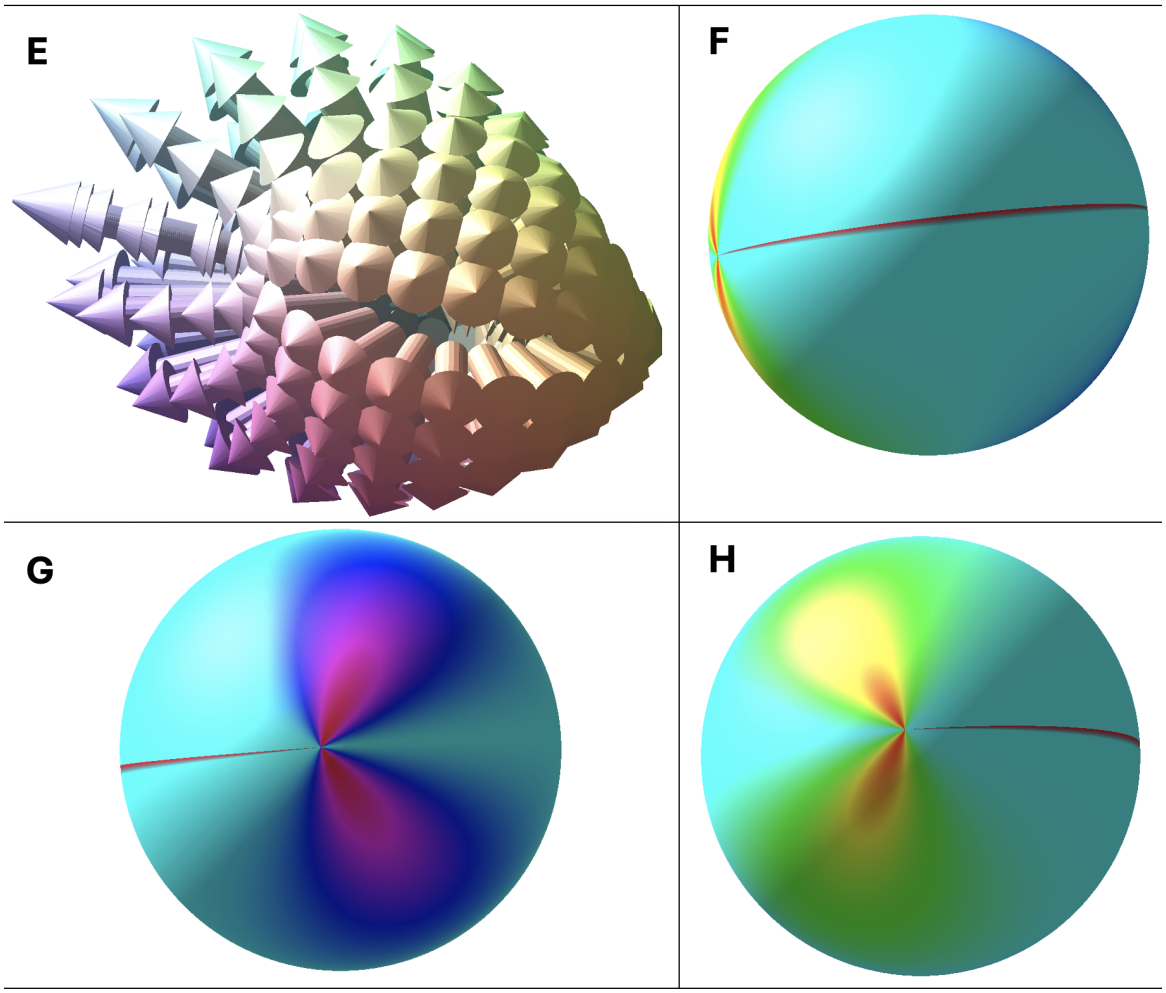

Figure 10. Figure 10 is the 3D phase plot of the emitted forward-backward peaking bremsstrahlung radiation with non-normalised vector length. Radiation phase is demonstrated on 3D spherical surface. Figure 10E is the combined top and bottom halves of the spherical phase vector in figure 9. Figure 10F-G is the different presentation of the 3D phase on a spherical surface. Phases are color coded. Figure 10G shows the forward, bottom half of the spherical surface and Figure 10H shows the top half, backward direction of the spherical surface. More importantly, red line connecting both bottom half phase rotation to top half phase rotation is the matching proof of current model to the previous model presented in Figure 5 and Figure 8 where spiral rotation starts at the front direction and rotation moves to the backward direction. Figure 10F with the red line across exactly shows that transition of rotation from forward to backward directions.

Figure 10F-G is a phase color coded 3D spherical presentation of the forward-backward peaking, asymmetric bremsstrahlung radiation phase pattern. Figure 10F-G proves the predictions of the previous model predictions presented in Figure 5 and Figure 8 where the spiral rotation starts at the front direction and the rotation moves to the backward direction. Figure 10F with the red line across shows the transition of rotation from forward to backward directions.

7 Discussion and Summary

Bremsstrahlung electron follows a spiral path under Earth's magnetic field, and combined with the curved trajectory arising from Coulomb interaction with other target particles during the bremsstrahlung process, this causes bremsstrahlung asymmetry to occur. The Bremsstrahlung asymmetry is also the property of twisted helical wavefront radiation.

Bremsstrahlung Radiation Pattern with twisted Helical Wavefront displays refractive gradients, turbulence, and ground reflections. They have significant azimuthal phase structure and azimuthal phase dependence around a center.

Significant azimuthal phase structure means the phase of the wave depends on the angle around a center point, not just on distance in one direction. That dependence is what reveals a twisted (OAM) wavefront in radio data.

Significant azimuthal phase structure is the tell-tale sign that the wavefront is not planar but has a helical twist or other structured geometry.

Let's imagine a circle of antennas arranged evenly around a center point. Each antenna measures the phase of the incoming wave. For a plane wave, the phase values across the circle form a straight gradient. On one side of the circle, all antennas see nearly the same phase. As we move across to the opposite side, the phase shifts smoothly. If phase vs. angle around the circle is plotted, we should get a flat or linear line.

On the other hand, let's imagine the same circle of antennas. For a twisted wave, the phase values change as you go around the circle. Instead of a straight gradient, the phase wraps around azimuthally. If phase vs. angle is plotted, we should see a spiral staircase pattern in which the phase increases steadily with angle.

Turbulence in the ionosphere, bremsstrahlung electrons with angular momentum can emit photons that carry OAM. This is a natural microscopic source of twisted light. These natural cases of twisted helical wavefront radiation tend to be messy and transient — not like the clean, stable twisted beams used in labs.

The connection between helical wavefront and observed coherency of lightning sferics could be that helical wavefront (corkscrew) across the beam of radiation ensures spatial coherence is preserved. Temporal coherence ensures that the twist does not fluctuate randomly over time. Without coherence, the helical structure would collapse into noise.

However, as can be seen in Figure 3, which is the curl plot describing the rotation of the wavefront of the bremsstrahlung emission, the radius of rotation decreases as the beam propagates, and the wavefront is not perfectly stable. Shrinkage of radius is irregular (different parts of the rotating wavefront collapse unevenly about the axis at zero radians), and the helical structure breaks down. That is a sign of reduced spatial coherence. This indicates and demonstrates more like emissions from a lightning, a lightning behaviour, and lightning sferics. Figure 3 shows that bremsstrahlung emissions start with a rotating wavefront, more like a tapered helical wavefront, and lose their spatial coherency as their helical structure breaks down due to irregular shrinkage of radius. This leaves radiation from the bremsstrahlung process with only temporal coherence. Temporal coherence in rotating wavefront and coherency in lightning sferics both describe time domain phase stability. This could explain why the lightning discharges display a temporal coherence but not spatial coherence, hence why lightning sferics are not known to produce structured wavefronts.

Preserved temporal coherence means the beam still has a stable frequency and phase over time, but without spatial coherence, the structured geometry is gone. Temporal coherency measures how stable the phase of a broadband lightning pulse is across multiple sensors. If the lightning pulse fluctuates randomly in time, coherency values drop, and interferometric mapping becomes less accurate. This remaining temporal coherency from the initial rotating tapered helical wavefront enables lightning interferometry.

Energy continuously flows azimuthally, but the phase surfaces may be stationary in time. A rotating wavefront requires the phase surfaces to move in the azimuthal direction with time.

7.1 Understanding Asymmetries

The position vector $r(t) = \frac{(t^R)^2 b^R (\omega')^R cos(\theta_{n,r(t)})^R c}{\tau^{2R} c^R \omega' cos(\theta_{n,r(t)})} - \frac{at}{\tau}$, from a paper describing bremsstrahlung asymmetry "Asymmetric Backward Peaking Radiation Pattern From a Relativistic Particle Accelerated by Lightning Leader Tip Electric Field" [26][p. 5, Eq. 1] does not incorporate and account for Doppler shift inside it.

It was interesting to predict and discover to see the Doppler shift asymmetry inside final equation 10, which relates multiples of the quantum of action, n, to the bremsstrahlung asymmetry,

R. This indicate the two asymmetries are related with each other, which is discussed little more in detail below.

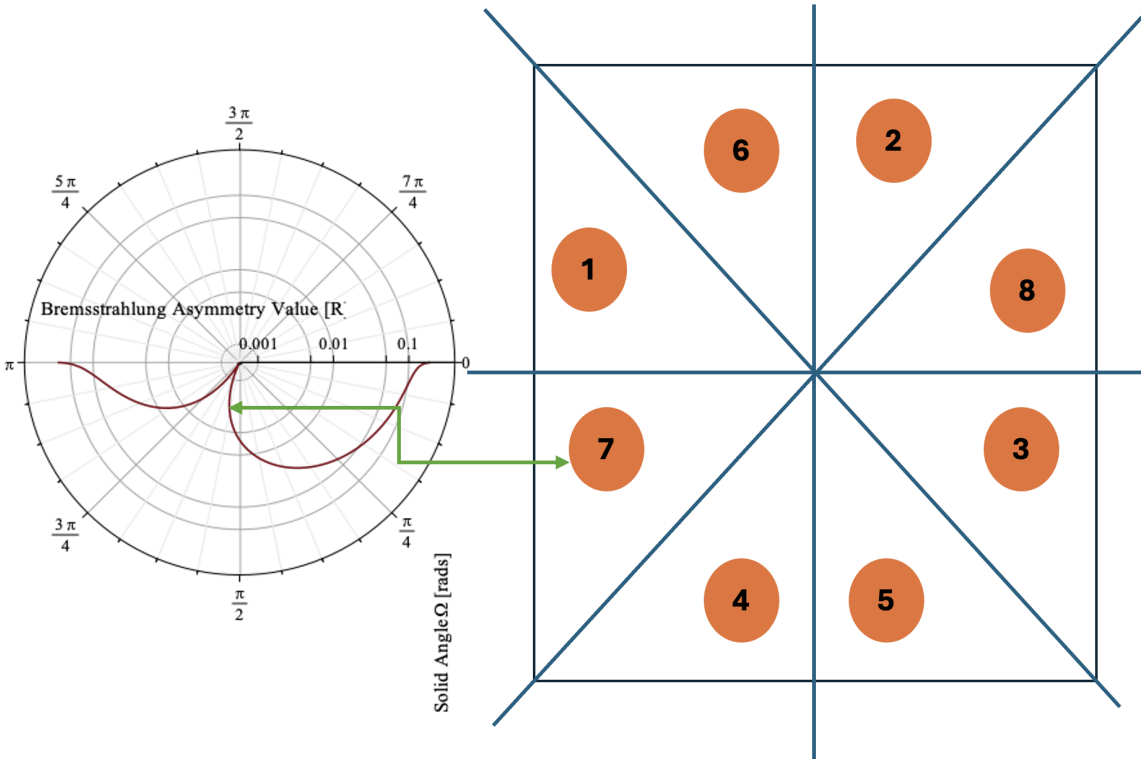

Figure 11. Conjecture for connected Bremsstrahlung and Doppler shift asymmetries. Orange circles are used to create asymmetries about the axes of symmetries of a square. If we pick one orange circle with any number and ignore all the others, we can see that wherever we position the orange circles to create asymmetry, we also cause asymmetries about other existing axes of symmetries of the system as well.

As shown in Figure 8 pattern 5, a conjecture for the reason why the Bremsstrahlung asymmetry does not go directly to zero at the angle $\pi/2$ is the Doppler shift asymmetry. We can see that the Doppler shift asymmetry and the Bremsstrahlung asymmetry are connected in this instance. In this case, particles have two lines of asymmetries for the emitted radiation. The vertical line of asymmetry for the Doppler shift and the horizontal line of asymmetry for the Bremsstrahlung asymmetry. As demonstrated with a rectangle shape example in Figure 11, regardless of where we put the orange circle (numbered from 1 to 7), we always affect all the other lines of asymmetries too, and the shape becomes asymmetric about all the available axes of symmetries. This means that once we create an asymmetry about one axis of symmetry of an object, we automatically create asymmetries about the other remaining axes of symmetry of the same object.

Common expected radiation patterns, such as low-frequency dipole radiation patterns and relativistic forward peaking radiation patterns existing in the literature [27, p. 669, Fig. 14.4], all demonstrate the existence of horizontal symmetry. The Doppler effect introduces the asymmetry about the vertical axis, and these two axes of symmetries were found to be related and work together. Since the horizontal axis of symmetry already exists, we know that if we break the symmetry around one axis of symmetry, which is due to the Doppler effect, hence this should mean breaking the symmetry around the horizontal axis too, which requires bremsstrahlung asymmetry, R to exist.

Figure 7 represents the forward-backward peaking radiation pattern of a high energy bremsstrahlung electron where the particle has two axes of symmetries, the vertical and horizontal axes passing through the origin. The Doppler effect on its own cannot create an asymmetry with respect to the horizontal axis of symmetry. Therefore, like in Figure 8, if we follow the conjecture or assumption that "if we create an asymmetry about one of the axes of symmetries of an object or particle, we cause an asymmetry in all of the existing axes of symmetries", this means Bremsstrahlung asymmetry must exist to do the work of creating an asymmetry about the horizontal axis of symmetry in emitted bremsstrahlung radiation patterns.

7.2 Shading or Circle Method in Creating Asymmetries

Each colour of shading or each circle represents one physics effect that causes symmetry breaking. For example, shading with yellow could represent "Doppler Effect" as a cause of breaking symmetry or alternatively, shading with "Grey". An important assumption is to assign one physical cause for each symmetry breaking. Either one colour shading or one circle.

Similarly, with the circle method, each circle represents one physical cause for each symmetry breaking. Putting the centre of the circle (or any geometry at the centre) right on the axes of symmetries of any object is the same as the shading method.

As can be seen in Figure 7, apart from the radiation being emitted by the particle at the origin, which is where the radiation patterns could meet the horizontal and vertical axes of symmetries. Radiation patterns never touch the horizontal and vertical axes of symmetries. Therefore, radiation patterns are never divided equally around the axes of symmetries.

This information can be used to assume that the circle method can be used to introduce asymmetry in the system involving radiation patterns and also to set a rule that circles used in introducing asymmetry cannot be placed on the axes of symmetries where center of the circle lies exactly on the axes of symmetries. This means that the use of the shading method can be eliminated in the modelling of introducing asymmetries into the system.

Table 2. Comparison of symmetry breaking by shading vs. placing a Circle.

Aspect	Shading (Global)	Circles like in figure 10 (Local)
Scale of change	Large area / whole region	Single point, a circle or small feature
Control	Can preserve chosen axes by aligning shading	Only preserves axes passing through the circle
Breaking effect	Partial: some axes survive, others break	Absolute: off-axis placement breaks all

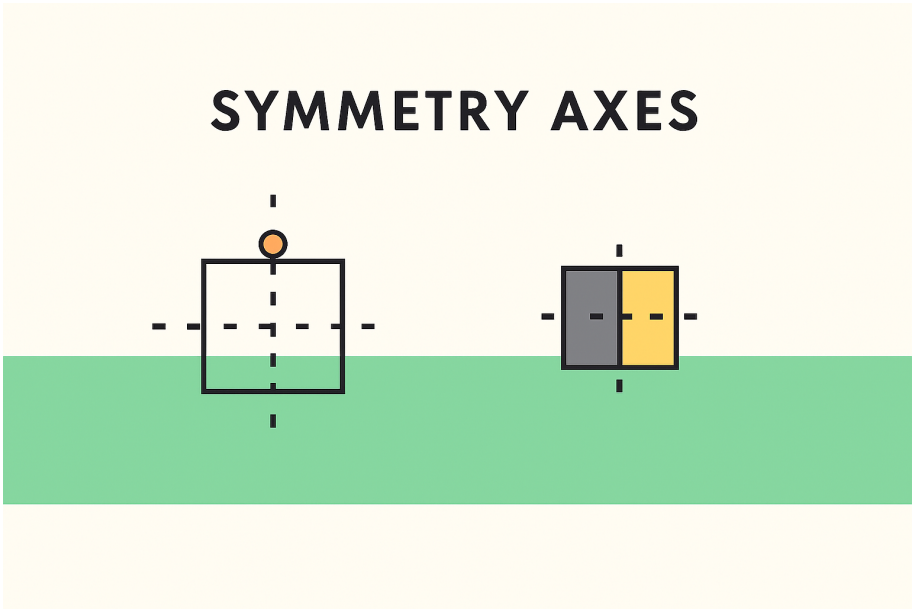

Figure 12. Symmetry breaking by shading demonstrate the existence of only horizontal axis of symmetry. Putting the center of the circle (or any geometry at the center) right on the axes of symmetries of any object is same as shading method.

All in all, this means that Doppler shift asymmetry and Bremsstrahlung asymmetry create each other during the Bremsstrahlung process. During the Bremsstrahlung process, when bremsstrahlung asymmetry occurs, it automatically creates an asymmetry about the vertical axis, which is the Doppler shift asymmetry. In systems where a particle on follows a straight trajectory, there is only one axis of symmetry, which is the Doppler shift about the vertical axis, hence it can only happen about the vertical axis. However, if we have more than one axis of symmetries, then creating an asymmetry about one axis means asymmetry about all the axis of symmetries of an object.

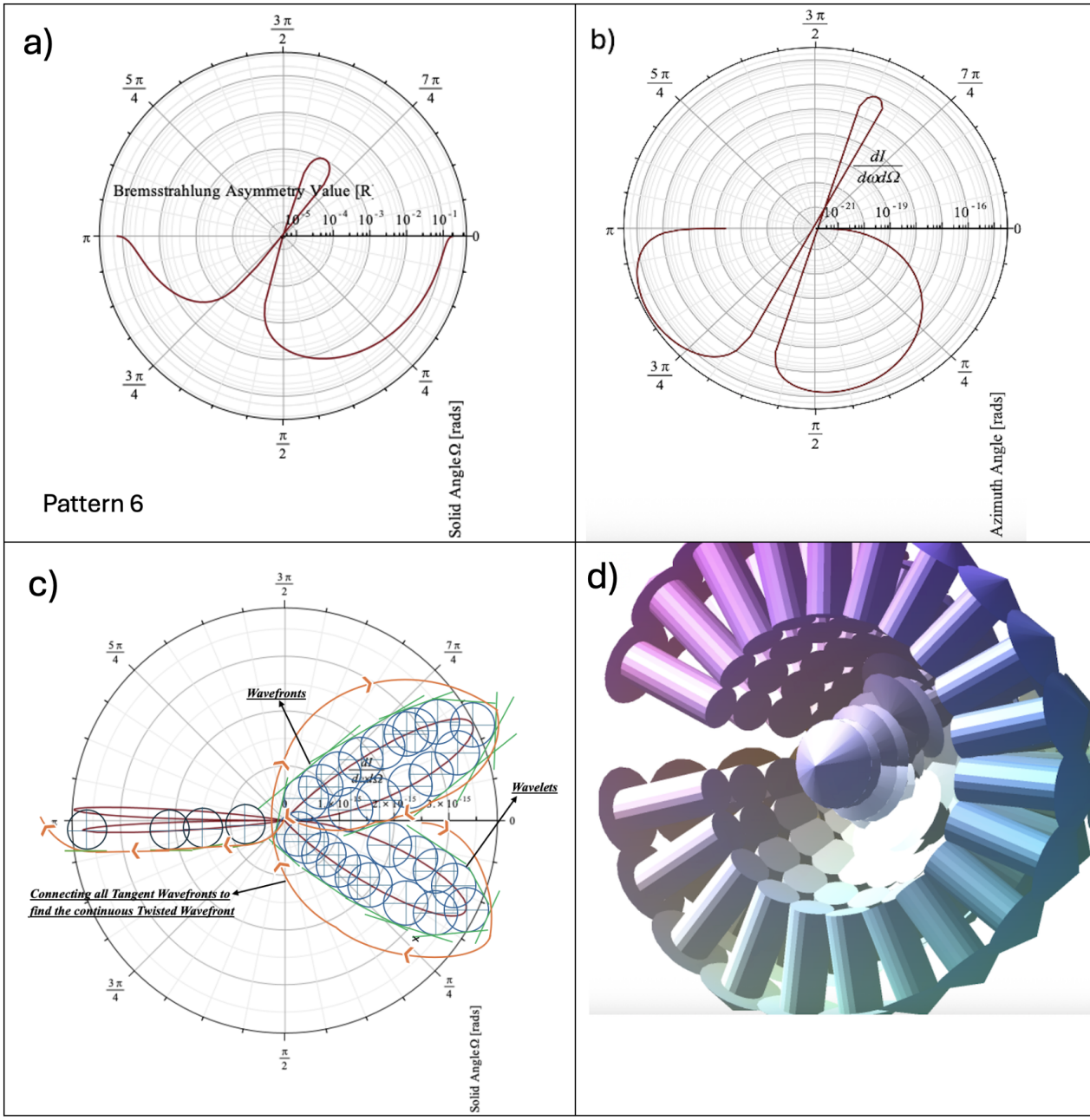

Figure 13. a) Pattern 6 is the prediction of quantized bremsstrahlung asymmetry, R(n), derived from momentum transfer from particle to rotating wavefront photon, quantized via conservation of momentum. Plot b) is the prediction of the curl of the gradient of the scalar radiation intensity field. c) is the prediction of Huygens' principle, which states that every point on a wavefront acts as a source of secondary spherical wavelets. Finally, d) Method that naturally extracts the phase of the wave from the radiation intensity pattern defined by equation 1 via decomposition of even denominator fraction defining bremsstrahlung asymmetry R. All in all, four different approaches converge to the same rotational wavefront. All four different methods show exactly the same rotational pattern.

The main highlights of this research are that the bremsstrahlung radiation was found to be first emitted as tapered helical wavefront propagation due to photon orbital angular momentum. Secondly, bremsstrahlung and Doppler shift asymmetries cause a variable radius, backward moving helix, and the radius of the rotational wavefront was found to be decreasing. Finally, Bremsstrahlung emissions become spatially incoherent as their tapered helical structure breaks down due to irregular shrinkage of radius.

Acknowledgments

I would like to thank my family for their support and good wishes.

Funding
This research received no specific grant from any funding agency in the public, commercial, or not-for-profit sectors.

Author contributions
The author carried out all aspects of the research and manuscript preparation.

Data availability
The Maple and Mathematica worksheets used to simulate the rotating wavefront of Bremsstrahlung process is openly available from Zenodo Research Data Archive at https://doi.org/10.5281/zenodo.18279338. The Maple worksheets used to simulate the particle bremsstrahlung asymmetry, R as a function of the integer multiple of quantum of action "n" is openly available from the University of Loughborough Research Data Archive at 10.17028/rd.lboro.29446097. The Maple worksheets for the simulation of novel 3D phase extension of the bremsstrahlung electromagnetic wavefronts is openly available from Zenodo Research Data Archive at https://doi.org/10.5281/zenodo.18695204. These simulations are the continuation of the previous Maple worksheets used to simulate the particle trajectory, external lightning leader tip electric field, particle velocity, and the radiation patterns which are openly available from the University of Bath Research Data Archive at https://doi.org/10.15125/BATH-00810.

References

[1] Padgett M 2024 *Philosophical Transactions of the Royal Society A: Mathematical, Physical and Engineering Sciences* **382** 20230327 ISSN 1364-503X (*Preprint* https://royalsocietypublishing.org/rsta/article-pdf/doi/10.1098/rsta.2023.0327/1329967/rsta.2023.0327.pdf) URL https://doi.org/10.1098/rsta.2023.0327

[2] Allen L, Padgett M and Babiker M 1999 Iv the orbital angular momentum of light (*Progress in Optics* vol 39) ed Wolf E (Elsevier) pp 291–372 URL https://www.sciencedirect.com/science/article/pii/S0079663808703913

[3] Ababekri M, Guo R T, Wan F, Qiao B, Li Z, Lv C, Zhang B, Zhou W, Gu Y and Li J X 2024 *Phys. Rev. D* **109**(1) 016005 URL https://link.aps.org/doi/10.1103/PhysRevD.109.016005

[4] Ababekri M, Zhou J L, Guo R T, Ren Y Z, Kou Y H, Zhao Q, Li Z P and Li J X 2024 *Phys. Rev. D* **110**(7) 076024 URL https://link.aps.org/doi/10.1103/PhysRevD.110.076024

[5] Karlovets D V 2012 *Phys. Rev. A* **86**(6) 062102 URL https://link.aps.org/doi/10.1103/PhysRevA.86.062102

[6] Wan C, Chen J, Chong A and Zhan Q 2021 *National Science Review* **9** nwab149 ISSN 2095-5138 (*Preprint* https://academic.oup.com/nsr/article-pdf/9/7/nwab149/45290666/nwab149.pdf) URL https://doi.org/10.1093/nsr/nwab149

[7] Hernández-García C, Picón A, San Román J and Plaja L 2013 *Phys. Rev. Lett.* **111**(8) 083602 URL https://link.aps.org/doi/10.1103/PhysRevLett.111.083602

[8] Seipt D, Surzhykov A and Fritzsche S 2014 *Phys. Rev. A* **90**(1) 012118 URL https://link.aps.org/doi/10.1103/PhysRevA.90.012118

[9] Vieira J, Trines R M G M, Alves E P, Fonseca R A, Mendonça J T, Bingham R, Norreys P and Silva L O 2016 *Phys. Rev. Lett.* **117**(26) 265001 URL https://link.aps.org/doi/10.1103/PhysRevLett.117.265001

[10] Chen Q, Qin H and Liu J 2017 *Scientific Reports* **7** 41731

[11] Katoh M, Fujimoto M, Mirian N S, Konomi T, Taira Y, Kaneyasu T, Hosaka M, Yamamoto N, Mochihashi A, Takashima Y, Kuroda K, Miyamoto A, Miyamoto K and Sasaki S 2017 *Scientific Reports* **7** 6130

[12] Wang W, Liu S, Lei S, Geng X, Shen B, Bu Z and Ji L 2022 *Phys. Rev. Res.* **4**(2) 023084 URL https://link.aps.org/doi/10.1103/PhysRevResearch.4.023084

[13] Bahrdt J, Holldack K, Kuske P, Müller R, Scheer M and Schmid P 2013 *Phys. Rev. Lett.* **111**(3) 034801 URL https://link.aps.org/doi/10.1103/PhysRevLett.111.034801

[14] Takabayashi Y, Takeda H, Magome E, Sumitani K, Kazinski P O, Korolev P S, Bogdanov O V and Tukhfatullin T A 2025 *Phys. Rev. A* **111**(6) L061501 URL https://link.aps.org/doi/10.1103/gxwj-yvdj

[15] Epp V, Guselnikova U and Janz J 2026 *Journal of Physics B: Atomic, Molecular and Optical Physics* **59** 015401 URL https://doi.org/10.1088/1361-6455/ae340e

[16] Khare K, Lochab P and Senthilkumaran P 2020 *Orbital Angular Momentum States of Light* 2053-2563 (IOP Publishing) ISBN 978-0-7503-2280-5 URL https://doi.org/10.1088/978-0-7503-2280-5

[17] Swartzlander G A 2001 *Opt. Lett.* **26** 497–499 URL https://opg.optica.org/ol/abstract.cfm?URI=ol-26-8-497

[18] Harwit M 2003 *The Astrophysical Journal* **597** 1266 URL https://doi.org/10.1086/378623

[19] Liu Z, Koh K L, Mezentsev A, Enno S E, Sugier J and Fullekrug M 2018 *Radio Science* **53** 448–457 (*Preprint* https://agupubs.onlinelibrary.wiley.com/doi/pdf/10.1002/2017RS006451) URL https://agupubs.onlinelibrary.wiley.com/doi/abs/10.1002/2017RS006451

[20] Füllekrug M, Liu Z, Koh K, Mezentsev A, Pedeboy S, Soula S, Enno S E, Sugier J and Rycroft M J 2016 *Geophysical Research Letters* **43** 10,448–10,454 (*Preprint* https://agupubs.onlinelibrary.wiley.com/doi/pdf/10.1002/2016GL070737) URL https://agupubs.onlinelibrary.wiley.com/doi/abs/10.1002/2016GL070737

[21] Said R K, Inan U S and Cummins K L 2010 *Journal of Geophysical Research: Atmospheres* **115** (*Preprint* https://agupubs.onlinelibrary.wiley.com/doi/pdf/10.1029/2010JD013863) URL https://agupubs.onlinelibrary.wiley.com/doi/abs/10.1029/2010JD013863

[22] Liu Z, Koh K L, Mezentsev A, Enno S E, Sugier J and Füllekrug M 2016 *Radio Science* **51** 1806–1815 (*Preprint* https://agupubs.onlinelibrary.wiley.com/doi/pdf/10.1002/2016RS006058) URL https://agupubs.onlinelibrary.wiley.com/doi/abs/10.1002/2016RS006058

[23] Bai X and Füllekrug M 2022 *Radio Science* **57** e2021RS007347 e2021RS007347 2021RS007347 (*Preprint* https://agupubs.onlinelibrary.wiley.com/doi/pdf/10.1029/2021RS007347) URL https://agupubs.onlinelibrary.wiley.com/doi/abs/10.1029/2021RS007347

[24] Bai X and Füllekrug M 2023 *Remote Sensing* **15** ISSN 2072-4292 URL https://www.mdpi.com/2072-4292/15/7/1950

[25] Yucemoz M 2022 *ESS Open Archive* URL https://essopenarchive.org/users/523129/articles/599209-spiral-radiation-pattern-of-a-relativistic-charged-particle-in-a-periodic-moti

[26] Yücemöz M and Füllekrug M 2021 *Journal of Geophysical Research: Atmospheres* **126** e2020JD033204 e2020JD033204 2020JD033204 (*Preprint* https://agupubs.onlinelibrary.wiley.com/doi/pdf/10.1029/2020JD033204) URL https://agupubs.onlinelibrary.wiley.com/doi/abs/10.1029/2020JD033204

[27] Jackson J D 1999 *Classical Electrodynamics* (New York, United States: John Wiley & Sons, Inc.) pp 661–732 3rd ed ISBN:9780471309321